Sensors & Actuators: B. Chemical 353 (2022) 131157

Contents lists available at ScienceDirect

Sensors and Actuators: B. Chemical

journal homepage: www.elsevier.com/locate/snb

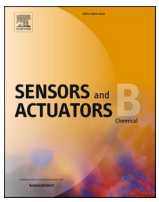

Localised plasmonic hybridisation mode optical fibre sensing of relative humidity

LiangLiang Liu, Serhiy Korposh, David Gomez, Ricardo Correia, Barrie R. Hayes-Gill, Stephen P. Morgan *

Optics and Photonics Group, Faculty of Engineering, University of Nottingham, Nottingham NG7 2RD, U.K

ARTICLE INFO

Keywords:
Optical fibre sensor
LSPR
Plasmonic hybridisation
Humidity sensor

ABSTRACT

This work reports an optical fibre probe functionalised with 'cotton-shaped' gold-silica nanostructures for relative humidity (RH) monitoring. The sensor response utilises the localised surface plasmon resonance (LSPR) of self-assembled nanostructures: gold nanospheres (40 nm) surrounded by one layer of poly (allylamine hydrochloride) and hydrophilic silica nanoparticles (10–20 nm) on the end-facet of an optical fibre via a wavelength shift of the reflected light. Sensor optimisation is investigated by varying the density of gold nanoparticles on the end-facet of an optical fibre. It is demonstrated that the plasmonic hybridisation mode appearing when the average gold interparticle distance is small (Median: 7.5 nm) is more sensitive to RH after functionalisation than the singular plasmonic mode. The plasmonic hybridisation mode sensor demonstrates a high linear regression to RH with a sensitivity of 0.63 nm/%RH and excellent reversibility. The response time ($T_{10–90\%}$) and recovery time ($T_{90–10\%}$) are calculated as 1.2 ± 0.4 s and 0.95 ± 0.18 s. The sensor shows no measurable cross-talk to temperature in the tested range between 25 °C to 40 °C and the 95% limit of agreement is 3.1%RH when compared to a commercial reference sensor. Simulation with finite element analysis reveals a polarisation-dependent plasmonic hybridisation with a redshift of plasmonic wavelength as a decrease of the interparticle distance and a higher refractive index sensitivity, which results in a high sensitivity to RH as observed in the experiment.

1. Introduction

Localised surface plasmon resonance (LSPR) is the resonance that occurs on a noble metal nanostructure with intense and highly confined electromagnetic fields, enabling high sensitivity to the surrounding refractive index (RI) and so is particularly attractive for sensing [1–4]. Sensing by utilising hybridisation phase of LSPR is previously reported to detect monolayers of biological molecules in which arrays of gold nanoantennas are sputtered on a thin layer of Si substrate and an open space lens system is adapted for the optical detection [5]. However, we believe that the sensor demonstrated in this paper is the first demonstration of an optical fibre sensor based on the plasmonic hybridisation mode of the LSPR.

Measurement of relative humidity (RH) is used as an exemplar. Different approaches have been investigated for relative humidity (RH) monitoring that build on the evolution of optical sensing mechanisms (e.g. evanescent field, reflectance, gratings, interferometers, resonators, lossy mode resonances, plasmonic sensing) as well as novel materials (e.g. polymers, hydrogel and nanoparticles) [6,7]. Among these, measurements based on a change in the wavelength of the reflected light such as from an optical grating are considered more robust for practical implementation than measurement of the intensity as the latter may be susceptible to the intensity drift of the light source and the external environment. The sensor demonstrated in this paper excites LSPR on the distal end of an optical fibre with 'cotton-shape' metal-dielectric nanoparticles. RH is measured through a change of RI induced by the interaction between water molecules and the hydrophilic dielectric nanocoating (silica nanoparticles, 20 nm) surrounding the gold nanospheres (40 nm). It is demonstrated that the plasmonic hybridisation mode due to near-field coupling between closely located AuNPs exhibits a higher RH sensitivity after the functionalisation with silica nanoparticles. Finite element analysis is conducted for studying the underlying physics of the plasmonic effect focusing on the plasmonic hybridisation between closely located gold nanoparticles, which theoretically supports the experimental observation. The proposed sensor demonstrates a fast response time, high accuracy with no measurable

* Corresponding author.
E-mail address: steve.morgan@nottingham.ac.uk (S.P. Morgan).

https://doi.org/10.1016/j.snb.2021.131157
Received 13 August 2021; Received in revised form 22 November 2021; Accepted 23 November 2021
Available online 27 November 2021

crosstalk over the tested temperature range and has the potential to be applied in healthcare.

Fibre optic LSPR sensors that use an optical fibre as a waveguide with metal nanostructure coated on its surface for excitation of LSPR, have previously been employed for biosensing [8,9]. However, there are relatively few examples that implement LSPR for humidity sensing [10–12] and among them only [10,12] use optical fibre sensing. It was reported that no significant wavelength shift was observed for the LSPR attenuation band for RH sensing when applying multi-layer silver nanoparticles loaded polymers [10] and a relatively low sensitivity of 0.04 nm/%RH for gold nanoparticles (AuNPs) [12]. Both of these were constructed with film depositions on the middle section of a cladding removed or stripped optical fibre. In this paper, we demonstrate the highest sensitivity (0.63 nm/%RH) of the wavelength shift based LSPR RH sensor by excitation of plasmonic hybridisation mode on the tip of an optical fibre for the first time.

2. Material and methods

2.1. Materials

Gold chloride trihydrate ($HAuCl_4$), sodium citrate dihydrate, 3-Aminopropyltriethoxysilane (APTES), poly (allylamine hydrochloride) (PAH, Mw~ 17500), Sulfuric acid (H_2SO_4) are purchased from Merck. Hydrogen peroxide (H_2O_2, >30% w/v) is purchased from Fisher Scientific. Silica Nanoparticles (SiNPs, 10–20 nm) are purchased from Tokyo Chemical Industry.

2.2. Sensor fabrication

The end facet of a silica optical fibre pigtail (62.5/125 μm, All4fibre) is firstly hydrolysed in freshly prepared Piranha solution (H_2SO_4:H_2O_2 =3:1 (v/v)) for 1 h at room temperature followed by washing with deionised water and drying under N_2 (washing and drying process). This is followed by immersion into 2% v/v APTES in ethanol for 20 mins and washing with deionised water and ethanol afterwards. This step creates amine active groups (-NH_2) on the fibre surface via the silanisation process. The fibre is subsequently sonicated in ethanol for a few seconds to remove the potential polymerised APTES layer and dried in an oven at 120 °C for 20 mins to condense the siloxane bond and remove water molecules from the surface.

Gold nanospheres (AuNPs, ~40 nm) are synthesized via the Turkevich method [13]: 1 mL of 12.7 mM sodium citrate dihydrate water solution is added into 39 mL of freshly prepared 0.325 mM gold chloride water solution while boiling, keeping boiling until the colour of the solution completely turns to red then cooling the solution in ambient temperature (~20 ^{0}C). The hydrodynamic size of the AuNPs is measured with dynamic light scattering (DLS, Nano-ZS, Malvern Instruments), the absorption spectrum of the AuNPs suspension is measured within a standard sample cuvette.

The silanised optical fibre is then immersed in the prepared AuNPs suspension for between 15 mins and 100 mins to obtain different quantities of AuNPs on the surface. After washing and drying, the AuNPs coated fibre tip is immersed into a positively charged polymer solution (PAH, 0.17 wt% in water) for 10 mins and subsequently immersed into negatively charged SiNPs (1 wt% in water) for a further 10 mins after washing and drying. A thin layer of PAH links to the AuNPs surface so that SiNPs can adsorb on the gold surface through electrostatic interaction [14]. The sensor is then ready to be used after washing and drying to remove unbounded SiNPs. The above coating process is illustrated in Fig. 1a. Sensors made with different immersion times are prepared via the same deposition process to investigate the effects of particle separation.

2.3. Sensing mechanism

The AuNPs have collective oscillation of electrons on the surface once irradiated by light at the resonance frequency, named the localised surface plasmon. The plasmon resonance frequency is sensitive to the local RI and a change in RI results in a shift of the resonance frequency. Well separated AuNPs on a substrate such as an optical fibre can sense the RI but multiple AuNPs at a close distance have different spectral properties and an enhanced RI sensitivity due to the near-field plasmonic coupling and plasmonic hybridisation [3,15,16]. A hot spot with enhanced electric field inbetween lead to the high fraction of light interaction with sensing element enabling high sensitivity. This is further confirmed from the simulation results in Section 3.4. On the other hand, SiNPs have unreacted silanol groups (Si-OH) on the surface and an inner mesoporous skeleton structure that can interact with water molecules via a weak hydrogen bond interaction leading to an increase of the RI when humidity changes. The constructed optical fibre sensor with composite nanostructure (Fig. 1b) on the fibre tip is therefore sensitive to RH. Notably, Fig. 1b is a simplified structure showing only a single particle, the near field coupling between AuNPs is not illustrated.

2.4. Experimental set-up

As illustrated in Fig. 1d(L), a climatic chamber (CVMS Climatic, Benchtop C-TH40) that controls relative humidity (± 2.5%RH) and temperature (fluctuation: ± 0.5 °C) is used for sensor characterisation. The nanoparticles functionalised sensing head of the fibre optic sensor (FOS) is placed inside the chamber with the pigtail connector of the fibre cable connected to a 2 × 1 multimode optical fibre coupler (Newport, F-CPL-M12855) via an ST (straight tip) connector that allows the easy exchange of the sensor and renders a disposable sensing head (Fig. 1c). A halogen light source (HL-2000, Ocean Insight) and a CCD spectrometer (Flame, Ocean Insight) are used for transmitting light to the sensing head and receiving the spectral response, respectively. Due to limitations of the climatic chamber in achieving RH< 50%, a flow set-up (Fig. 1d(R)) is implemented [17]. Different levels of RH are produced by regulating humidified and dry nitrogen gas with certain mixture volume ratios through two gas flowmeters. The FOS is positioned in a flow cell under the flow system for monitoring the humidity response.

2.5. Experimental procedure

For characterising the RH response of the FOS, the climatic chamber is programmed to increase and decrease RH step-by-step by 5% in the range between 50% and 90% at a fixed temperature of 25 °C. Spectra of the FOS are recorded dynamically during the process. The chamber is set to increase temperature likewise from 25 °C to 40 °C at a constant humidity (RH=55%) for investigation of temperature cross-sensitivity. The testing of sensor response and recovery time are performed by feeding and extracting the sensing head in and out the chamber (humidity steady at 80%) from ambient. Sensors that are made with different protocols (i.e., different immersion time in AuNPs) are tested individually for RH response to find the optimal density and separation of AuNPs. The embedded RH sensor inside of the chamber is used as the reference sensor for calibration.

The morphology of the coating on the tip of an optical fibre is examined by the means of Scanning electron microscopy (JEOL, JSM-7100 F). The average interparticle distance is defined as the edge-to-edge distance between two neighbouring particles. Counting the number of particles and calculation of the interparticle distance is obtained with the particle analysis function of the imaging processing software: ImagJ.

2.6. Finite element analysis

The absorption extinction of the AuNPs at different interparticle

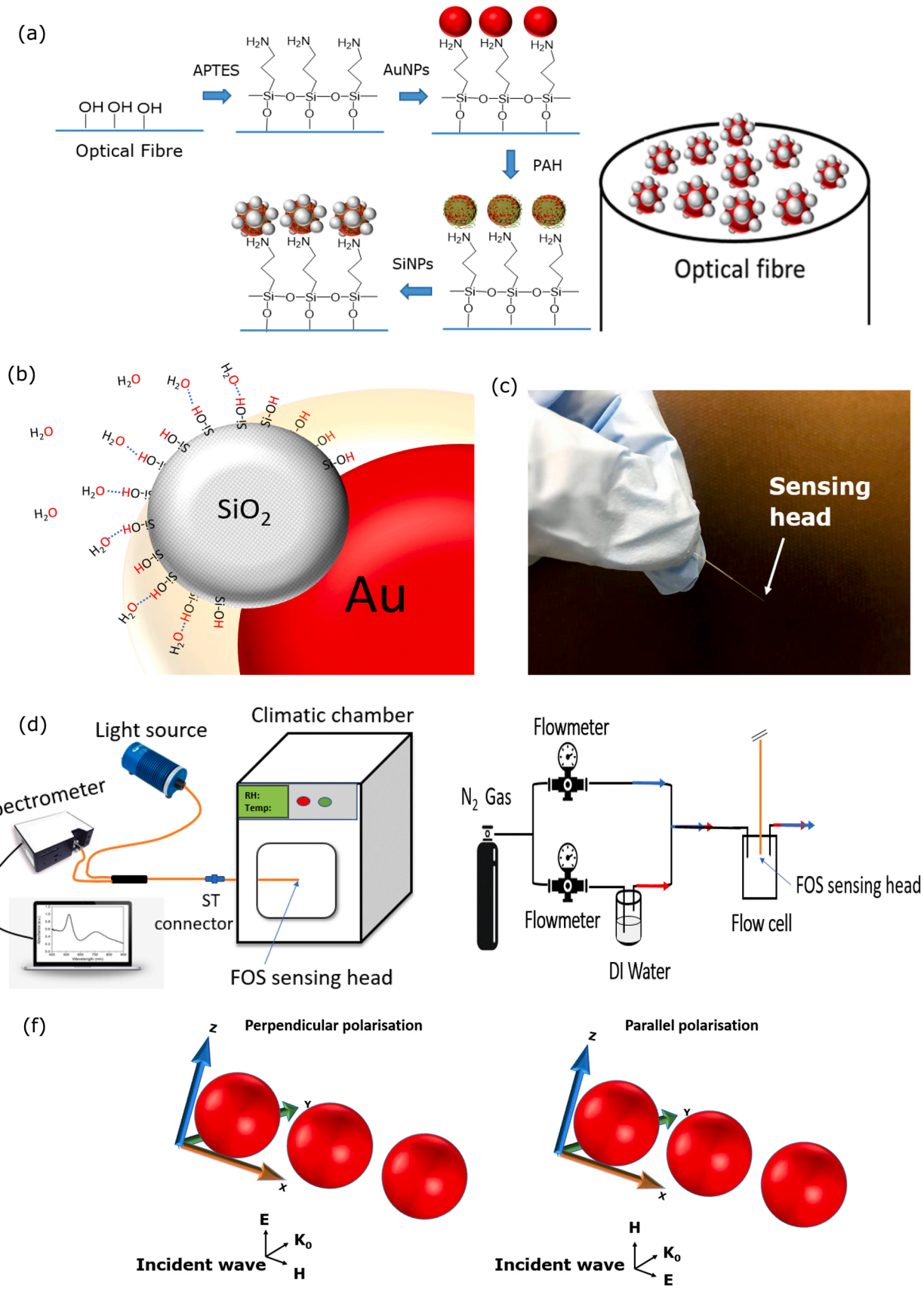

Fig. 1. (a) Schematic of surface functionalisation process on the tip of an optical fibre. (b) Schematic illustration of humidity sensing of the composite nanostructure. Note: Only one type of hydrogen bonding is shown in the graphic. (c) A picture of a fibre sensor. (d) The schematic set-up for sensor characterisation with RH> 50% (L) and RH< 50% (R). (f) Schematic of the simulation model: (L) perpendicular polarisation (R) parallel polarisation.

distances from 1 nm up to 50 nm are studied with 3D finite-element analysis based on commercial software COMSOL Multiphysics (Radio frequency module, Version 5.2). A simple AuNPs array (three identical AuNPs, Ø: 40 nm, illustrated in Fig. 1f) with identical interparticle distance is used as a simulation model for studying the interaction with an electromagnetic wave. We acknowledge the limitations of this approach considering the fact that the interparticle distances will not be identical in the real situation. However, it is able to demonstrate the trends observed experimentally. Two different polarisation directions of the incident light are chosen with one parallel to the array axis and the other perpendicular. The light beam is incident perpendicular to the array axis. The optical properties of gold are taken from the database of Johnson and Christy [18]. The detailed parameters setting regarding electromagnetic wave, boundary conditions, simulation domain and mesh size in COMSOL are referenced from the online tutorial material [19]. The radius of particles, scattering domain and perfectly matched layer (PML) are 20 nm, 150 nm, 200 nm respectively. The mesh size is $\lambda/8$ in the free space domain around the nanoparticles with a 3.3 nm (particle radius/6) element size for the particles. The absorption extinction value in the simulation is calculated as the integration of resistive loss of gold nanoparticles over input power as defined in [19].

3. Results

3.1. Sensor characterisation and optimisation

The average hydrodynamic size of the AuNPs is measured to be 40 nm according to the report from DLS and the size distribution is plotted in Fig. 2a. The AuNPs are later confirmed as having spherical shape from the observation of SEM with size agreeing with the DLS measurement (Fig. 2b).

Freely moving AuNPs in a solution bind covalently to the amine functionalised optical fibre surface during the immersion and the amount of AuNPs attached depends on immersion time. Fig. 3 shows SEM image of the AuNPs on the tip of an optical fibre for different immersion times. The number of particles that appear in the observed area (~2.2 μm^2) of an optical fibre for three different cases ((i) 15 mins, (ii) 45 mins and (iii) 100 mins) increases with reaction time (corresponding to the number of 157, 414 and 522 particles, respectively). The average interparticle distance decreases as a consequence of increasing of the number of AuNPs on the surface (Fig. 3b). AuNPs tend to randomly attach to the fibre so that the distribution in case (i) is broad and becomes narrow for higher reaction times once interparticle distance decreases (cases (ii) and (iii)). The absorbance due to light-particle interaction (or plasmonic effect) increases correspondingly (Fig. 3a). The plasmonic resonance wavelengths exhibit dependence on the interparticle distance with a blue shift for the absorption band as compared to the spectrum of gold suspension (532.6 6 1.2 nm, 523 6 0.4 nm, 519.7 6 0.7 nm (mean 6 standard deviation (SD)) with a sample volume of five) when interparticle distance decreases and this is considered to be dominated by the interaction of the orthogonal polarization of light with the interparticle axis of AuNPs as shown in later simulations (Fig. 8b) [16]. The blueshift is also observed during the immersion in the AuNPs suspension where the peak wavelength continuously shifts towards short wavelengths over the reaction time (result not shown). A second absorption band appears at a higher wavelength when interparticle distances are small (case (ii) and case (iii)), this is due to the plasmonic hybridization at the aggregation of nanoparticles for the interaction of parallel polarised light to the particle axis (confirmed from simulation results in Fig. 8a.b) [15,16]. The absorption spectrum contains two peaks as a result of a mixture of two polarisation states. Case (iii) is a more pronounced plasmonic hybridization mode with a much clearer 2nd band than case (ii) and is much easier for peak tracking. Fig. 3c shows the surface morphology of the tip of the FOS in which the small size SiNPs attached to the AuNPs surface forming 'cotton-shape' nanostructure on the surface of the fibre. It can be seen that SiNPs also attach to the free space of the fibre substrate due to the electrostatic interaction between the protonated amine groups from the silanisation process with negatively charged SiNPs.

After functionalisation with PAH/SiNPs, the spectrum of FOS (as shown in Fig. 4a) for case (i) has a wavelength shift of ~7 nm towards higher wavelength (red-shift), the spectrum of the case (ii) and (iii) however undergo a blue-shift for the first Peak with a magnitude shift of ~9 nm and ~ 13 nm, respectively. Fig. 4b demonstrates the wavelength response of the 1st absorption peak to different RH concentrations revealing higher sensitivity for case (iii) and almost no sensitivity for case (i). It is found in the latter case that the 2nd absorption peak (i.e. hybridization mode) has a significant response to RH as compared with the 1st peak. Therefore, the highest RH sensitivity for the reported sensing structure is with case (iii) and this sensing characterisation is shown in the remainder of the results section.

3.2. RH response of the optimised sensor

The optimised sensor spectrum (case (iii)) shows significant changes upon exposure to different levels of RH both in peak wavelengths and absorption (illustrated in Fig. 5a). In particular, the 2nd absorption peak shifts to a higher wavelength with increase of RH along with a decrease of absorption. The peak wavelength exhibits excellent repeatability when repeatedly exposed to the same RH (RH=80%) from the ambient condition (shown in Fig. 5b). The response time ($T_{10-90\%}$) and recovery time ($T_{90-10\%}$) is then calculated as 1.2 ± 0.4 s and 0.95 ± 0.18 s (mean ± SD). The dynamic change of the peak wavelength changes accordingly as the RH increases and decreases step-by-step (Fig. 5c). The wavelength demonstrates a linear relationship with the RH with a sensitivity of 0.63 nm/%RH (R^2 =0.98) for RH between 60% and 90% and a lower sensitivity for RH < 60% (Fig. 5d). In contrast, the wavelength of the 1st peak shifts to a lower wavelength with a sensitivity of − 0.03 nm/%RH

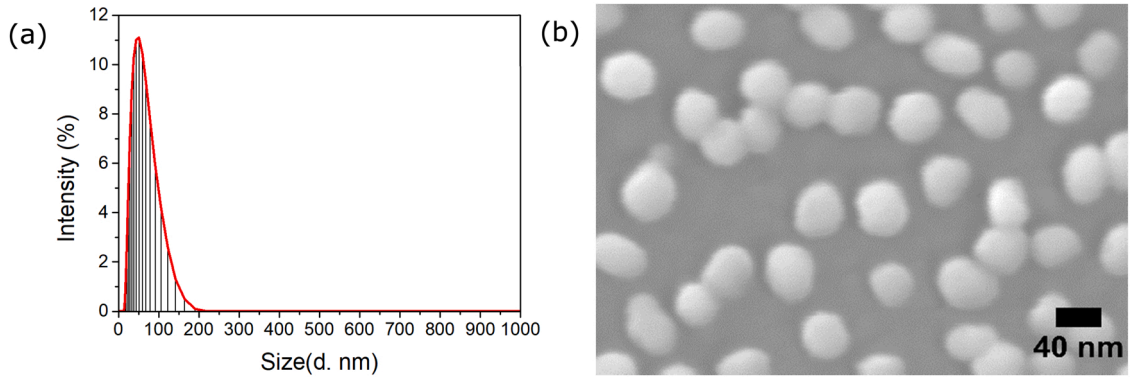

Fig. 2. (a) Size distribution of synthesised AuNPs, measurement from DLS. (b) SEM image of AuNPs (scale bar= 40 nm).

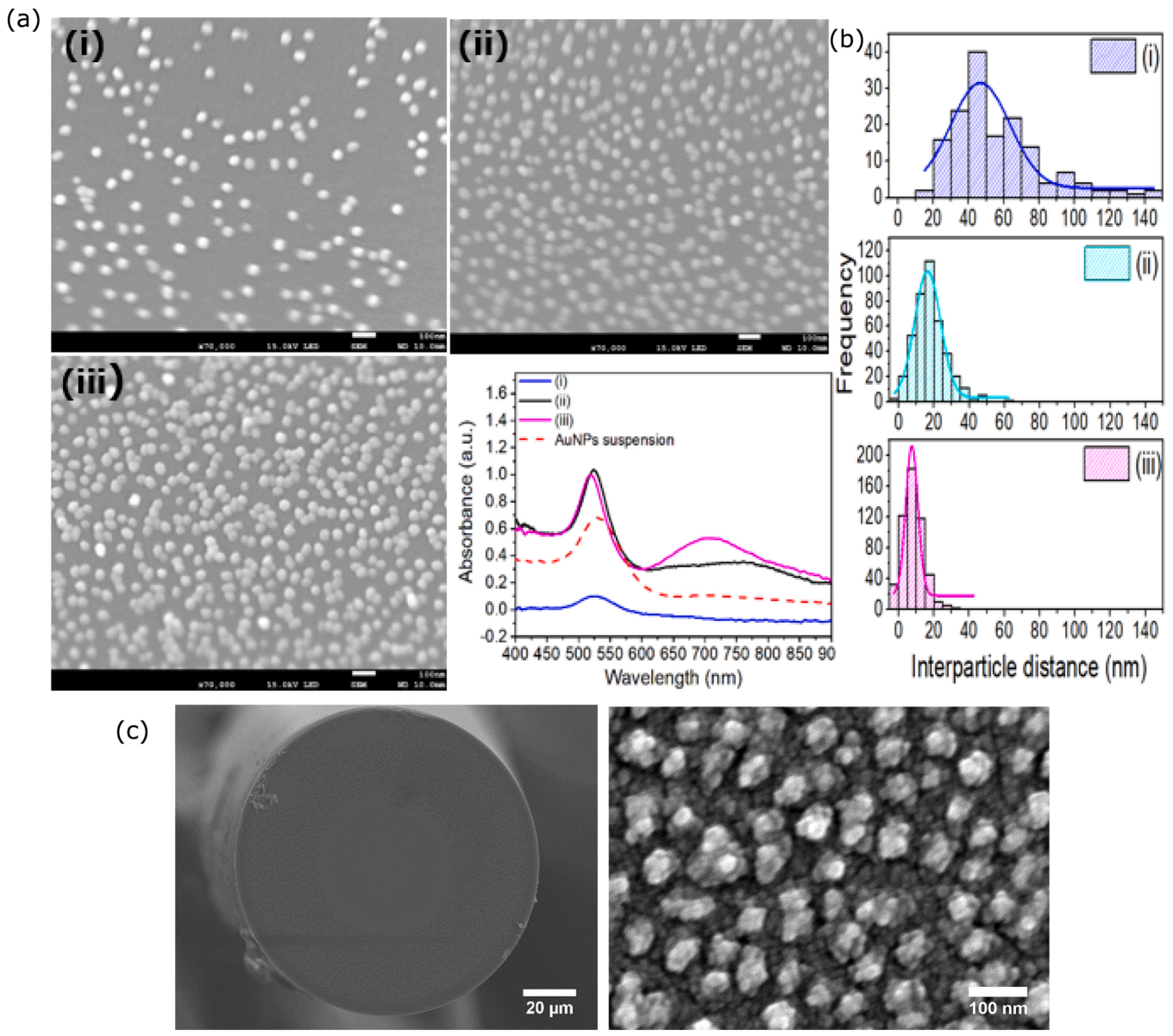

Fig. 3. (a) SEM images of the AuNPs on the tip of an optical fibre with different reaction time (i) 15 mins (ii) 45 mins (iii) 100 mins. Three images are taken under the same magnification (×70,000), and scale bars = 100 nm. The spectra are the absorption spectrum of the Au functionalised fibre and the spectrum of gold suspension for comparison. (b) The distribution of interparticle distance in the image in (a). (c) SEM image of a FOS RH sensor (L, scale bar= 20 μm) and the 'cotton-shape' nanostructure on the fibre surface (R, scale bar= 100 nm).

which is 21 times lower than the 2nd peak. The absorption value (taken from the 2nd peak) also shows a linear relationship with RH in the range of 60–90% and it decreases with increase of RH (Fig. 5e,f). A sensitivity of − 0.003/%RH is obtained (R^2 =0.99) in this range. The non-linear response at RH < 60% (Fig. 5d) is likely due to the climatic chamber operating close to its limit. As described in Section 2.4 a new set up was therefore implemented to investigate the response at the lower RH range (Fig. 1d(R)). A newly fabricated sensor exhibits a linear correlation across the tested RH range of 0–70% with a sensitivity of 0.65 nm/% RH (Fig. 5g) which is very close to the first one (Fig. 5f). This small performance variation maybe attributed to the variation in nanostructure introduced from the manufacturing process or systematic difference between the two calibration methods.

The calibrated FOS is further verified by measuring RH inside the chamber for another two consecutive cycles (RH: 60–90%) in comparison to the RH reading from the reference sensor. The results demonstrate that the FOS measures RH with a good agreement to the measurement of the reference sensor for different RH (Fig. 6a). The Bland-Altman plot is shown in Fig. 6b where each point is the difference between reading from the reference sensor and the FOS, taken from the steady RH of each stage in Fig. 6a. The 95% limit of agreement (LOA) is 3.1%RH with the mean difference or bias equals − 0.6% (Fig. 6b). Fig. 6c shows the RH measurement of the FOS in the programmed climate chamber on different days. This illustrates that the sensor maintains its performance after a week with a variation of reading to the reference value (red dashed lines) within the accuracy of the sensor measurement (defined as LOA: 3.1% RH).

3.3. Temperature cross-sensitivity

The cross-sensitivity of temperature is one important factor that needs to be considered and evaluated for a newly designed sensor. Fig. 7 shows the peak wavelength (2nd peak) of the FOS under different RH and temperature conditions. There is an outburst of RH when the

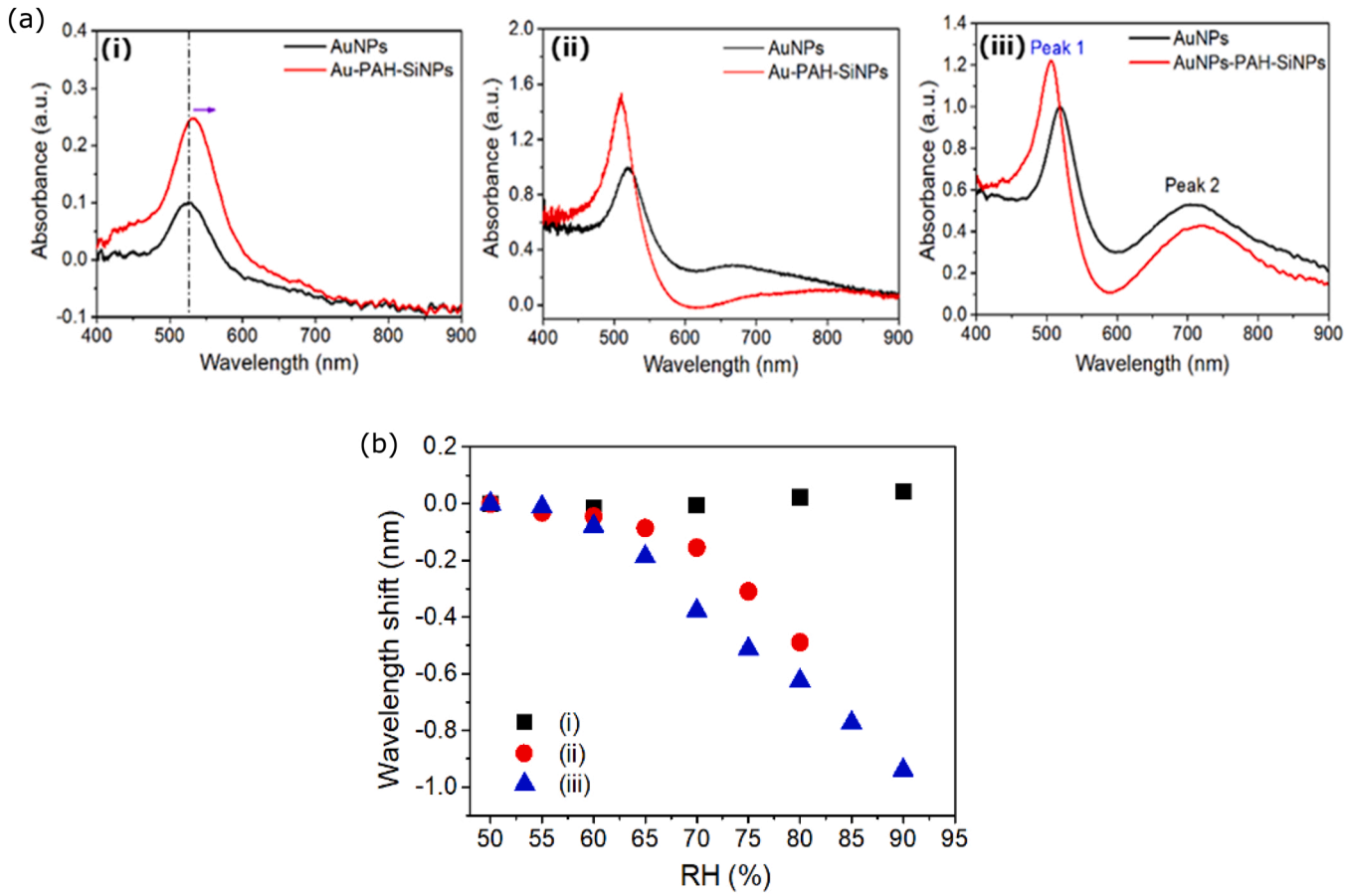

Fig. 4. (a) The spectral response of the three cases after functionalisation with one layer PAH/SiNPs. (b) RH sensitivity of sensors made in three cases. The 1st plasmonic peak was chosen for sensitivity comparison. Different immersion times are shown (i) 15 mins, (ii) 45 mins and (iii) 100 mins which affect the separation of the AuNPs.

temperature increase from 25 °C to 30 °C and it finally returns to its original setting (RH=55%) with the temperature remaining at 30 °C following an auto-adjustment of the chamber. The peak wavelength of the FOS follows the same trend and stabilises at the same value as it was at 25 °C. A similar performance occurred for temperatures up to 35 °C and 40 °C while RH remains at the same level. The wavelength shows a negligible change to temperature increase when the RH remain the same. The sensor is therefore considered temperature-insensitive for the range (25–40 °C).

3.4. *Finite element simulation of plasmonic hybridisation*

The simulated results show the absorption extinction is spectrally different depending on interparticle distances and polarisation of light (Fig. 8a,b). The light in parallel polarisation (Fig. 8a) has clear stronger interactions than the perpendicular polarisation (Fig. 8b) which agrees with the finding of Nordlander et al. [15] and such polarisation dependent spectral features are theoretically explained in [20]. For the parallel polarisation, a red-shift is observed when reducing the interparticle distance and a dual-peak appears when interparticle distance is extremely small as a result of the plasmonic hybridisation, similarly as observed in the experiment (Fig. 3a) and by others [16]. Prashant et al. explain the new peak in the shoulder (lower wavelength) is attributed to higher-order interactions possibly by quadrupole mode rather than the dipolar interaction model [16]. In contrast, there is a weak blueshift in response to decreasing interparticle distance for the perpendicular polarisation and this explains the observation in Fig. 3a where the plasmonic peak shifts to a shorter wavelength with higher immersion time. The plasmonic wavelength as a function of interparticle distance is shown in Fig. 8e where the red-shift and blue-shift are observed for different polarisations. This hybridisation mode of the higher wavelength band which is activated when interparticle distances are small (e.g. 1 nm) under parallel polarisation demonstrates a higher RI sensitivity of 282.4 nm/RIU than that of a large interparticle distance (e.g. 19 nm, 71 nm/RIU). The RI sensitivity shows an increase as a decrease of interparticle distance (Fig. 8f, black mark) and for a large interparticle distance (e.g. 50 nm), it is found to be proximal to the sensitivity of the single-particle alone (48 nm/RIU) (not shown). The interparticle distance, in this case, does not affect the sensitivity. However, for the perpendicular polarised light, the refractive index sensitivity shows a small decrease as the interparticle distance decreases.

4. Discussion

The reported nanostructure functionalised LSPR RH sensor relies on wavelength shift of the plasmonic resonance wavelength upon adsorption of water molecules on the sensing material (i.e. SiNPs). The highest sensitivity occurs at the plasmonic hybridisation mode where nanogaps between nanoparticles behave like hot spots with large field concentration leading to an enhancement of RI sensitivity. The enhancement of sensitivity for the RH sensing can also be attributed to the large sensing volume of the red-shifted plasmonic wavelength which renders a high penetration depth. It is desirable to have narrow plasmonic bands to obtain the best resolution and probably the highest sensitivity, which requires good control of nanogaps with great uniformity. The self-assembly method adopted in this work is a simple way of depositing nanoparticles but it is difficult to control precisely the nanogaps required to achieve a narrow band. Lithographic techniques can produce

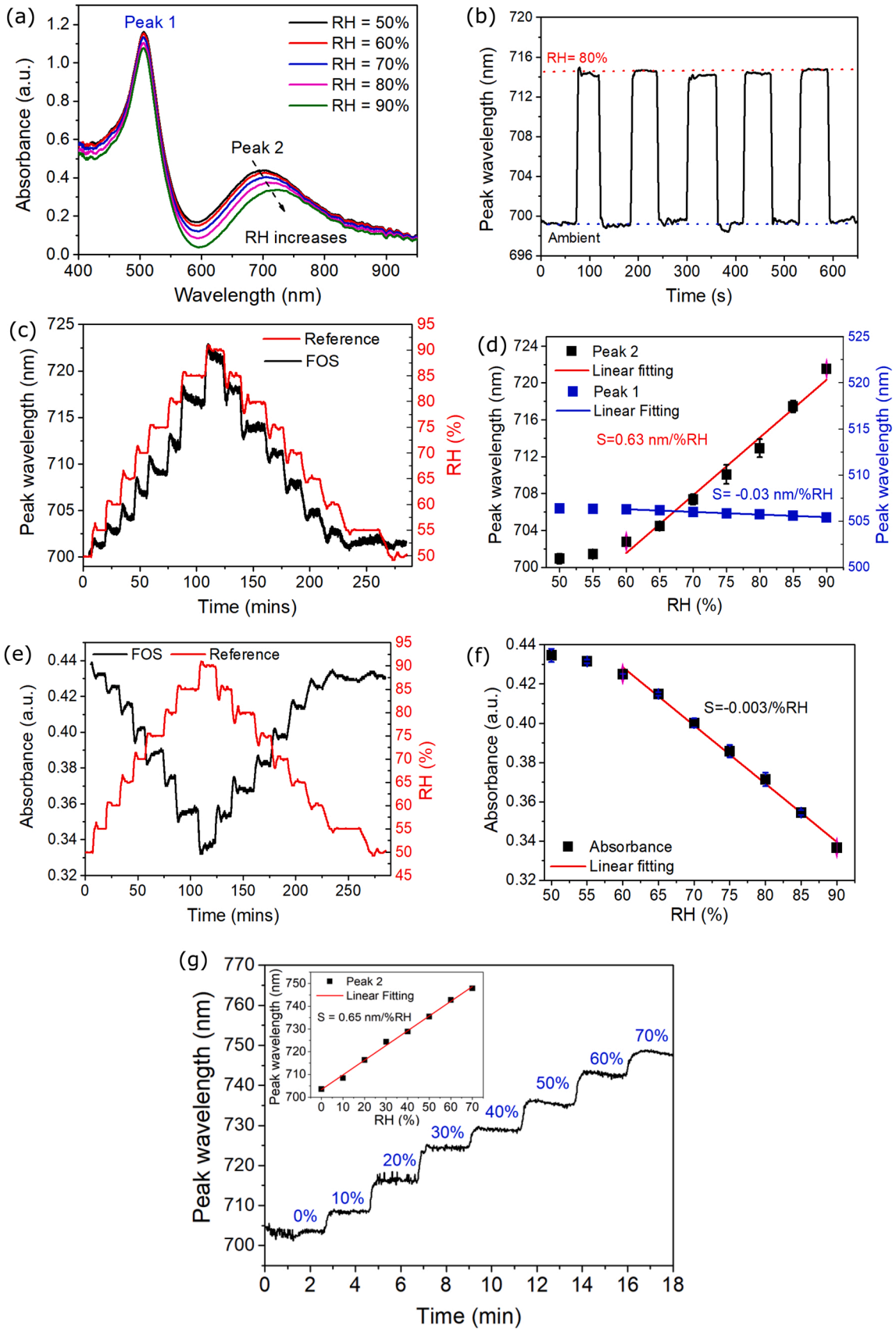

Fig. 5. (a) Spectral response of the FOS for different RH. (b) Repeatability test of the sensor to a constant RH (RH=80%). (c) The dynamic response of the FOS to RH. (d) Peak wavelengths of the FOS as a function of RH. (e) The absorbance of the peak wavelength change with RH. (f) Linear fitting of the absorbance value to RH. (g) An independent measurement of RH at a low RH by using set-up in Fig. 1d(R).

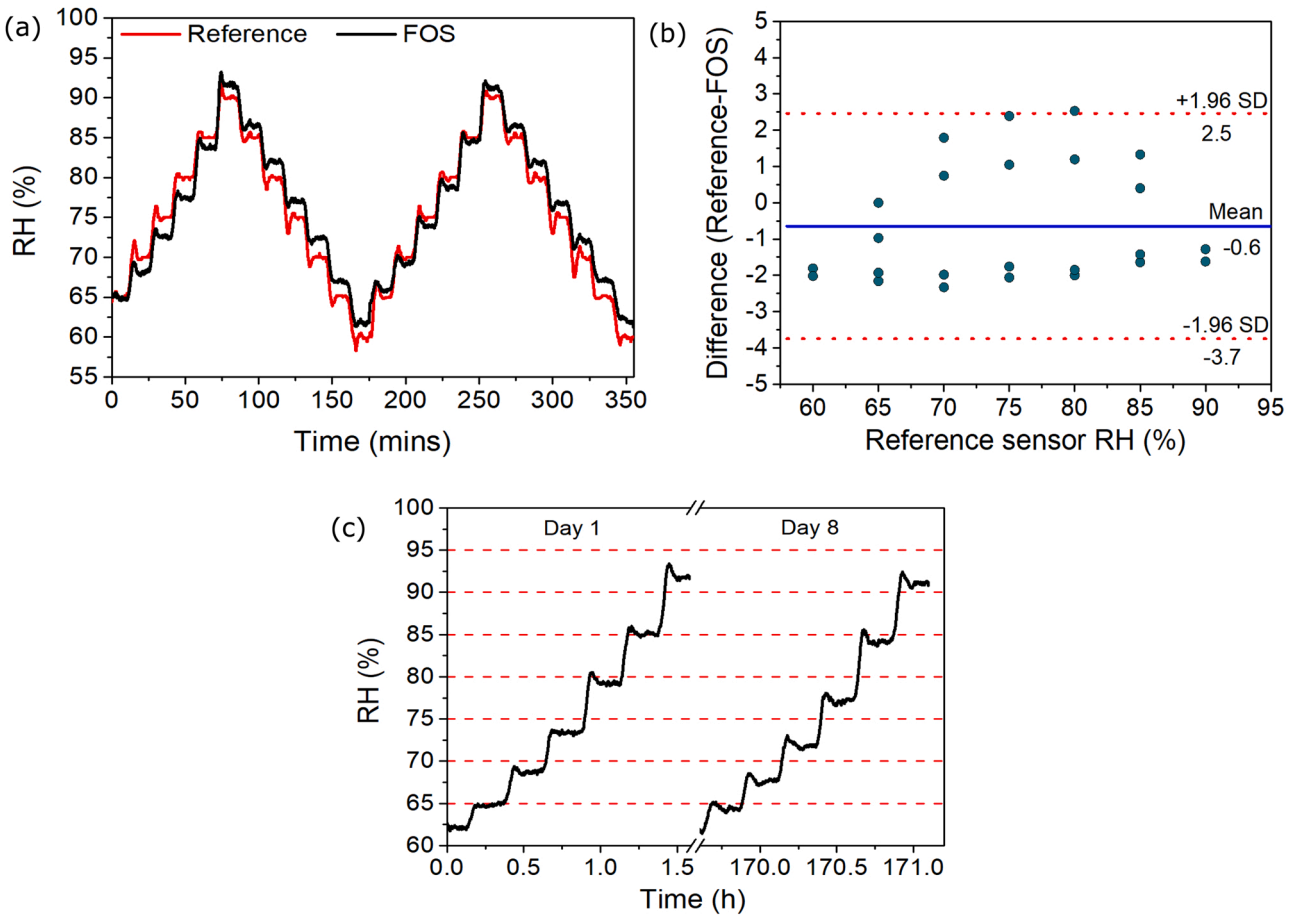

Fig. 6. (a) The measurement of RH with FOS in comparison to the reference sensor. (b) Bland-Altman plot of the FOS. (c) The measurement of RH over different days inside of the climate chamber.

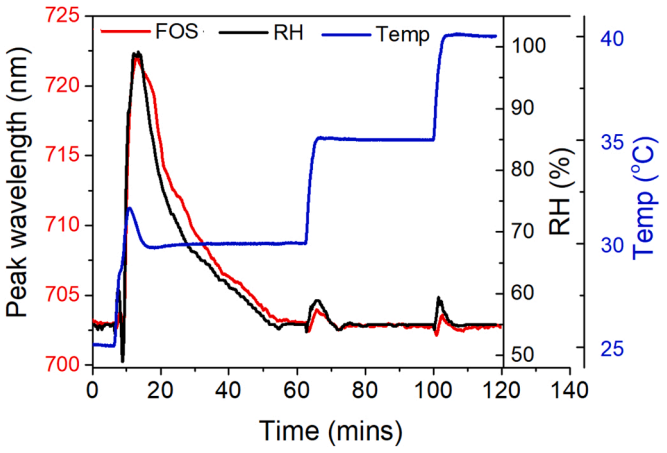

Fig. 7. Temperature cross-sensitivity test of the FOS.

a highly ordered pattern for particle deposition with the flexibility in the design of the nanogaps to achieve narrow plasmonic bands [21]. However, in many applications this may be too costly.

The spectral behaviour of the plasmonic hybridisation is polarisation dependent for the incident light as seen in simulation results in Fig. 8 and also reported by others [15,16]. This dependence can be explained using a simple dipole-dipole coupling model. The dipole-dipole interaction is attractive for parallel polarisation resulting in a reduction of plasmon frequency (red-shift) and repulsive for the orthogonal polarisation leading to an increase of the plasmon frequency (blue-shift) [22].

In this work, the light source is randomly polarised so that the absorption spectrum obtained is a mix of both polarisation states and distinctive features are seen in one spectrum. There is a clear blue shift in response to the PAH/SiNPs coating and RH measurement (an increase of local refractive index) when a high density of AuNPs appears on the surface (case (ii) and case (iii)). This cannot be explained by the simulation model and may be associated with the complex higher-order plasmonic interaction between multiple particles.

The key step for sensor fabrication is to have the optimum structure of nanoparticles on the fibre tip surface. Although the self-assembly of AuNPs does not produce structurally identical surfaces, the fabrication process is repeatable and results in distinctive spectral features (two absorption bands) being well matched between sensors (Fig. 9a) (variation of $\pm$ 0.05 nm and $\pm$ 1.7 nm for the 1st and 2nd peak, respectively).

To investigate the wavelength robustness of the sensor, the input light power is manipulated by mechanically controlling the optical shutter of the light source which increases or decreases the light input (mimicking light fluctuation). The result shows that the absorbance value changes accordingly as a result of changing the real-time input light while the normalisation still takes the initial input as a reference. The peak wavelength is, however, remains relatively stable (Fig. 9b) indicating that the wavelength-based measurement is more tolerant to the intensity-based measurement.

Measurement of humidity plays a significant role in healthcare such as in monitoring the microenvironment of a clinical wound [23] and the air delivery to mechanically ventilated patients in critical care [24]. It is widely accepted that moisture balance is important for optimum wound healing and too moist or too dry microenvironments should be avoided [23,25,26]. Effective management of wound moisture can shorten the

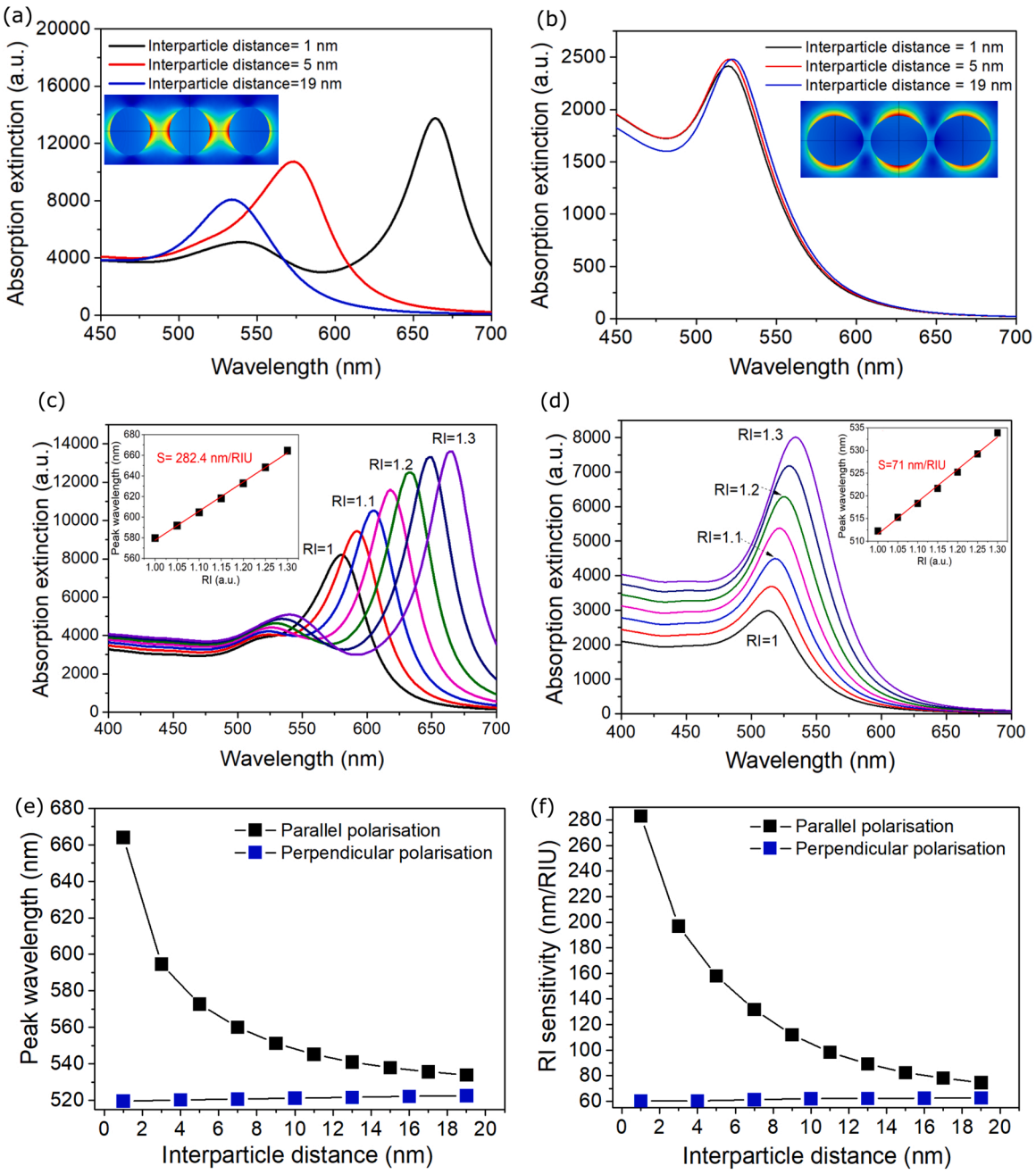

Fig. 8. The extinction spectrum for the simulated AuNPs array of different interparticle distances with (a) parallel polarisation and (b) perpendicular polarisation (RI = 1.3). The extinction spectrum under different RI for the parallel polarisation with an interparticle distance of (c) 1 nm and (d) 19 nm, corresponding sensitivities are 282.4 nm and 71 nm, respectively. (e) The plasmonic peak wavelength at different interparticle distances for the two polarisations. (f) The RI sensitivity as a function of interparticle distance for the two polarisations.

healing time and the frequency of dressing change, which in turn reduces nursing time and patient visiting. However, the determination of an optimal moist healing environment relies on good clinical judgements which are subjective, and treatment may sway from the actual needs, such as changing the dressings while the wound is still in its optimum moisture range. Measurement of humidity in the wound microenvironment is less invasive than the state of the art (Woundsense sensor) which measures the moisture level electrically with silver chloride electrodes embedded in a porous film upon contact with wound exudates [27]. For mechanical ventilation of a patient, or other breathing apparatus such as continuous positive air pressure (CPAP) or a nebuliser, adequate humidification of inspired gases is important to avoid the hazards associated with under-humidification in which dry gases can lead to a sequence of respiratory functional impairment particularly for the mucociliary elevator [28]. Monitoring the humidity level of the inspired gases would enable the management of humidification and supply of optimal ventilation condition to patients.

FOS can satisfy every requirement of healthcare monitoring including high sensor performance and biocompatible features [29,30], which have led to great interest in healthcare [31,32]. The small diameter of the FOS (typically a hundred microns) meets the needs of real-time monitoring in a compact space such as within a wound dressing close to the wound microenvironment [17] or within the lumen of an endotracheal tube [33] without adversely interfering with existing clinical procedures. Moreover, the optical sensing feature renders immunity to electromagnetic interference allowing the application of FOS

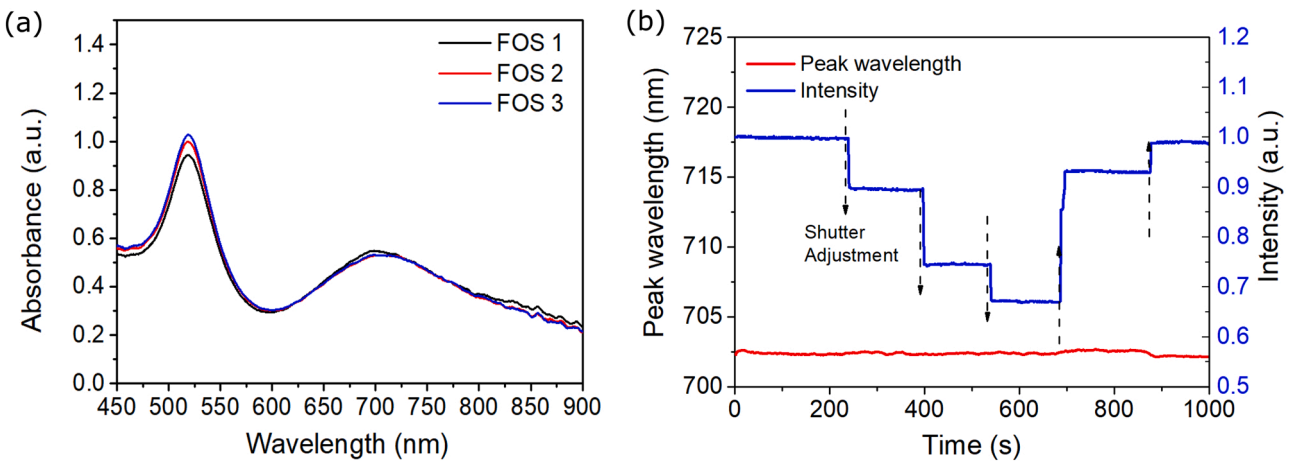

Fig. 9. (a) Absorption spectrum of the AuNPs functionalised fibre sensor. (b) The signal change during light modulation. The intensity value is normalised with its initial value when the shutter is fully opened (i.e. I_1/I_0; I_i: intensity is under monitoring, I_0: the intensity when the shutter is fully opened).

in the healthcare environment where stringent electromagnetic compatibility (BS60601–1–2) is required, even allowing for instance, monitoring during MRI scanning [34].

5. Conclusion

A fibre optic RH probe is reported utilising plasmonic hybridisation between coupled gold nanoparticles with nanostructure functionalised fibre tip. This is the first time that the LSPR hybridisation mode has been used as an optical fibre sensing mechanism. Its sensing capability is demonstrated for RH after functionalisation with hydrophilic SiNPs forming 'cotton-shaped' nanostructure on the end facet. The sensor exhibits a linear relationship between plasmonic wavelength and RH with a sensitivity of 0.63 nm/RH for the range of 60–90% RH. The sensor is demonstrated with a Bland Altman limits of agreement measurement accuracy of 3.1% (bias −0.6%) compared to the reference commercial sensor. It has a fast response time of 1.2 ± 0.4 s and recovery time of 0.95 ± 0.18 s and exhibits no temperature cross-sensitivity in the tested range of 25–40 °C. The sensor also shows good stability and reliability over measurement on different days. It is demonstrated experimentally and theoretically that the optimal sensor is with a high density of gold nanoparticles on the sensor surface with plasmonic hybridisation between coupled gold nanoparticles which renders a high refractive index sensitivity and a potentially large sensing volume.

CRediT authorship contribution statement

Liu: Conceptualisation, Methodology, Software, Validation, Formal analysis, Investigation, Writing – original draft. **Correia:** Methodology, Validation, Investigation, Writing – review and editing, Supervision, Funding acquisition. **Gomez:** Methodology, Validation, Investigation, Writing – review and editing. **Korposh:** Conceptualisation, Methodology, Writing – review and editing, Supervision, Funding acquisition. **Hayes-Gill:** Validation, Writing – review and editing, Supervision, Funding acquisition. **Morgan:** Conceptualisation, Writing – review and editing, Supervision, Project administration, Funding acquisition.

Declaration of Competing Interest

The authors declare that they have no known competing financial interests or personal relationships that could have appeared to influence the work reported in this paper.

Acknowledgements

This work was supported by the Development Pathway Funding Scheme of The Medical Research Council (UK, MR/R025266/1). SPM is funded by a Royal Society Industry Fellowship.

References

[1] B. Sepúlveda, P.C. Angelomé, L.M. Lechuga, L.M. Liz-Marzán, LSPR-based nanobiosensors, Nano Today 4 (2009) 244–251.
[2] K.M. Mayer, J.H. Hafner, Localized surface plasmon resonance sensors, Chem. Rev. 111 (2011) 3828–3857.
[3] E. Martinsson, B. Sepulveda, P. Chen, A. Elfwing, B. Liedberg, D. Aili, Optimizing the refractive index sensitivity of plasmonically coupled gold nanoparticles, Plasmonics 9 (2014) 773–780.
[4] C. He, L. Liu, S. Korposh, R. Correia, S. Morgan, Volatile Organic Compound Vapour Measurements Using a Localised Surface Plasmon Resonance Optical Fibre Sensor Decorated with a Metal-Organic Framework, Sensors 21 (2021) 1420.
[5] R.R. Gutha, S.M. Sadeghi, C. Sharp, W.J. Wing, Biological sensing using hybridization phase of plasmonic resonances with photonic lattice modes in arrays of gold nanoantennas, Nanotechnology 28 (2017), 355504.
[6] J. Ascorbe, J.M. Corres, F.J. Arregui, I.R. Matias, Recent developments in fiber optics humidity sensors, Sensors 17 (2017) 893.
[7] T.L. Yeo, T. Sun, K.T.V. Grattan, Fibre-optic sensor technologies for humidity and moisture measurement, Sens. Actuators A: Phys. 144 (2008) 280–295.
[8] J. Cao, M.H. Tu, T. Sun, K.T.V. Grattan, Wavelength-based localized surface plasmon resonance optical fiber biosensor, Sens. Actuators B: Chem. 181 (2013) 611–619.
[9] H.-Y. Lin, C.-H. Huang, G.-L. Cheng, N.-K. Chen, H.-C. Chui, Tapered optical fiber sensor based on localized surface plasmon resonance, Opt. Express 20 (2012) 21693–21701.
[10] P.J. Rivero, A. Urrutia, J. Goicoechea, F.J. Arregui, Optical fiber humidity sensors based on Localized Surface Plasmon Resonance (LSPR) and Lossy-mode resonance (LMR) in overlays loaded with silver nanoparticles, Sens. Actuators B: Chem. 173 (2012) 244–249.
[11] Z.-m Qi, I. Honma, H. Zhou, Humidity sensor based on localized surface plasmon resonance of multilayer thin films of gold nanoparticles linked with myoglobin, Opt. Lett. 31 (2006) 1854–1856.
[12] R. Aneesh, S. Khijwania, Localized Surface Plasmon Resonance based optical fiber humidity sensor with etched fiber core comprising enhanced sensitivity, 2012 International Conference on Fiber Optics and Photonics (PHOTONICS)2012, pp. 1–3.
[13] J. Kimling, M. Maier, B. Okenve, V. Kotaidis, H. Ballot, A. Plech, Turkevich method for gold nanoparticle synthesis revisited, J. Phys. Chem. B 110 (2006) 15700–15707.
[14] L. Liu, L. Marques, R. Correia, S.P. Morgan, S.-W. Lee, P. Tighe, L. Fairclough, S. Korposh, Highly sensitive label-free antibody detection using a long period fibre grating sensor, Sens. Actuators B: Chem. 271 (2018) 24–32.
[15] P. Nordlander, C. Oubre, E. Prodan, K. Li, M.I. Stockman, Plasmon hybridization in nanoparticle dimers, Nano Lett. 4 (2004) 899–903.
[16] P.K. Jain, W. Huang, M.A. El-Sayed, On the universal scaling behavior of the distance decay of plasmon coupling in metal nanoparticle pairs: a plasmon ruler equation, Nano Lett. 7 (2007) 2080–2088.
[17] D. Gomez, S.P. Morgan, B.R. Hayes-Gill, R.G. Correia, S. Korposh, Polymeric optical fibre sensor coated by SiO2 nanoparticles for humidity sensing in the skin microenvironment, Sens. Actuators B: Chem. 254 (2018) 887–895.

[18] P.B. Johnson, R.-W. Christy, Optical constants of the noble metals, Phys. Rev. B 6 (1972) 4370–4379.
[19] Y.R. Davletshin, COMSOL Practice, Finite element calculation of the optical properties of plasmonic nanoparticles, Ryerson University (2016). Available at ⟨www.researchgate.net/profile/Yevgeniy-Davletshin/publication/311103297_COMSOL_Practice_Finite_element_calculation_of_the_optical_properties_of_plasmonic_nanoparticles/links/583dce5808ae2d217554c360/COMSOL-Practice-Finite-element-calculation-of-the-optical-properties-of-plasmonic-nanoparticles.pdf⟩. (last accessed 20th Nov 2021).
[20] Y.-F. Chou Chau, C.M. Lim, C. Lee, H.J. Huang, C.-T. Lin, N.T.R.N. Kumara, V. N. Yoong, H.P. Chiang, Tailoring surface plasmon resonance and dipole cavity plasmon modes of scattering cross section spectra on the single solid-gold/gold-shell nanorod, J. Appl. Phys. 120 (2016), 093110.
[21] V. Kravets, F. Schedin, A. Grigorenko, Extremely narrow plasmon resonances based on diffraction coupling of localized plasmons in arrays of metallic nanoparticles, Phys. Rev. Lett. 101 (2008), 087403.
[22] S.A. Maier, M.L. Brongersma, P.G. Kik, H.A. Atwater, Observation of near-field coupling in metal nanoparticle chains using far-field polarization spectroscopy, Phys. Rev. B 65 (2002), 193408.
[23] G.D. Winter, Formation of the scab and the rate of epithelization of superficial wounds in the skin of the young domestic Pig, Nature 193 (1962) 293–294.
[24] F.U. Hernandez, S.P. Morgan, B.R. Hayes-Gill, D. Harvey, W. Kinnear, A. Norris, D. Evans, J.G. Hardman, S. Korposh, Characterization and use of a fiber optic sensor based on PAH/SiO 2 film for humidity sensing in ventilator care equipment, IEEE Trans. Biomed. Eng. 63 (2016) 1985–1992.
[25] S.M. Bishop, M. Walker, A.A. Rogers, W.Y. Chen, Importance of moisture balance at the wound-dressing interface, J. Wound care 12 (2003) 125–128.
[26] G. Schultz, D. Mozingo, M. Romanelli, K. Claxton, Wound healing and TIME; new concepts and scientific applications, Wound Repair Regen. 13 (2005) S1–S11.
[27] S.D. Milne, I. Seoudi, H. Al Hamad, T.K. Talal, A.A. Anoop, N. Allahverdi, Z. Zakaria, R. Menzies, P. Connolly, A wearable wound moisture sensor as an indicator for wound dressing change: an observational study of wound moisture and status, Int. Wound J. 13 (2016) 1309–1314.
[28] M. Shelly, G. Lloyd, G. Park, A review of the mechanisms and methods of humidification of inspired gases, Intensive care Med. 14 (1988) 1–9.
[29] R. Nazempour, Q. Zhang, R. Fu, X. Sheng, Biocompatible and implantable optical fibers and waveguides for biomedicine, Materials 11 (2018) 1283.
[30] Z. Tang, D. Gomez, C. He, S. Korposh, S.P. Morgan, R. Correia, B. Hayes-Gill, K. Setchfield, L. Liu, A U-shape fibre-optic pH sensor based on hydrogen bonding of ethyl cellulose with a sol-gel matrix, J. Light. Technol. 39 (2021) 1557–1564.
[31] R. Correia, S. James, S. Lee, S. Morgan, S. Korposh, Biomedical application of optical fibre sensors, J. Opt. 20 (2018), 073003.
[32] A.G. Leal-Junior, C.A. Diaz, L.M. Avellar, M.J. Pontes, C. Marques, A. Frizera, Polymer optical fiber sensors in healthcare applications: a comprehensive review, Sensors 19 (2019) 3156.
[33] R. Correia, R. Sinha, A. Norris, S. Korposh, S. Talbot, F. Hernandez, et al., Optical fibre sensing at the interface between tissue and medical device, SPIE,, 2017.
[34] P. Polygerinos, A. Ataollahi, T. Schaeffter, R. Razavi, L.D. Seneviratne, K. Althoefer, MRI-compatible intensity-modulated force sensor for cardiac catheterization procedures, IEEE Trans. Biomed. Eng. 58 (2010) 721–726.

LiangLiang Liu is a research fellow working in the Optics and Photonics Group, University of Nottingham, UK. His research interest is to develop implantable photonics sensing devices for disease monitoring and interaction of neural activities

Serhiy Korposh received both his bachelor and master degrees in 2001 and 2002 respectively in physics from Uzhgorod National University, Transcarpathia (Ukraine) and Ph.D. degree from Cranfield University in 2007. He worked as a post-doctoral researcher on development of the novel materials for chemical sensors in the Graduate School of Environmental Engineering of the University of Kitakyushu from 2008 to 2012. From 2012–2013 he worked as a research fellow in the Department of Engineering Photonics, Cranfield University. Since 2013 he is an Associate Professor at the University of Nottingham. His research interest lies in the field of development of fibre-optic chemical sensors modified with the sensitive materials and their applications in healthcare and environmental monitoring.

Ricardo Goncalves Correia is an assistant Professor in Optical Fibre Sensing at the University of Nottingham. As an Instrumentation Engineer specialised in the development of fibre optic sensors, his research passion focusses on the development and application of fibre optic sensors for a wide range of applications that range from healthcare to civil engineering and aerospace. His main interest is in the development and application of fibre optic sensors for physical measurements.

Barrie Hayes-Gill is Professor of Medical Devices and Electronic Systems at the University of Nottingham. His research covers a broad range of the application of electronic engineering and optical systems to medical devices with an emphasis on technology transfer. Some of his recent work has involved the deployment of an optical sensor in a newborn's cap to monitor heart rate and oxygen saturation at birth along with the deployment of fibre optic sensors in wearable medical devices in both hospital and home settings. Most significantly he has developed a wearable fetal monitor for mothers at birth which is now being deployed in thousands of births around the world. He is a Chartered Engineer and Fellow of the Institution of Engineering Technology.

Stephen Morgan is Professor of Biomedical Engineering at the University of Nottingham. His research involves the development of devices to monitor the microcirculation specifically in tissue breakdown and wound healing. For example, he currently developing a novel endotracheal tube that can monitor the microcirculation at the cuff/trachea interface. Recent work involves the development of photonic textiles. These sensing systems, incorporated into garments can monitor pressure, temperature, the microcirculation and other biomarkers. His work has involved close collaboration with numerous industry partners. He is a Royal Society Industry Fellow and Academic Director of the Centre for Healthcare Technologies which aims to bring together key stakeholders, capabilities and expertise to support the rapid translation of scientific discoveries into healthcare adoption.